

Synthetic Hertzsprung-Russell diagrams of open clusters

Lionel Siess, Manuel Forestini, and Catherine Dougados

Laboratoire d'Astrophysique, Observatoire de Grenoble, Université Joseph Fourier, BP 53, F-38041 Grenoble Cedex 9, France

Received 22 July 1996 / Accepted 28 January 1997

Abstract. New evolutionary models for pre-main sequence (PMS) stars ($0.4M_{\odot} \leq M \leq 5M_{\odot}$) of three different metallicities ($Z = 0.005$, $Z = 0.02$, and $Z = 0.04$) have been computed. Improvements have been made in the constitutive physics with the use of new opacity tables at low temperatures and new atmospheric models. We first compare our mass tracks with other recent PMS models and show that important deviations occur below $0.5M_{\odot}$, due to different treatments of the electrostatic corrections in cool degenerated matter. We first check the ability of our models to reproduce the ZAMS location and the low-mass end of the isochrones. From the turn-off in the M_V versus (B-V) diagram, we estimate ages of $4 \cdot 10^7$ yr for α Per cluster and between $8 \cdot 10^7$ and 10^8 yr for the Pleiades, ages comparable or lower than recent determinations including overshooting.

These evolutionary models are used to generate synthetic Hertzsprung-Russell Diagrams (HRD). We show that each of the different parameters, namely the initial mass function (IMF), the star formation rate (SFR) and the binary fraction affect in a specific way the morphology of the derived HRD. We propose to use these synthetic diagrams to constrain some of these quantities in observed open clusters. Applying this procedure to the Pleiades cluster, the observed morphology is best reproduced by invoking a large age dispersion ($\sigma_t \simeq 3 \times 10^7$ yr) and a binary fraction for F-G stars of $40\% \pm 5\%$.

Key words: stars: evolution of - stars: pre-main sequence - stars: Hertzsprung-Russell diagram - stars: fundamental parameters

1. Introduction

Since the founder publication of Iben (1965), many works have been devoted to the study of the pre-main sequence evolutionary phase. From that time, the constitutive physics to be included in stellar models has been significantly improved (see Sect. 2.1.1). As mentioned by several authors (Mazzitelli 1989; Forestini 1994 and hereafter F94; D'Antona & Mazzitelli 1994, hereafter DM94) many uncertainties still remain in this field. Effects engendered by various treatments of surface conditions or differ-

ent convection models influence the location of the tracks and isochrones in the HRD.

During its PMS phase, a star undergoes a quasi static contraction that will end with the onset of central hydrogen burning. Its structure remains fully convective along the almost vertical Hayashi track and rapidly turns radiative at the center where the opacity decreases with increasing temperature. The important nucleosynthetic events during this early phase sum up in deuterium, lithium and beryllium depletions. Apart during the short deuterium burning phase, the energetics is supplied by the gravitational contraction until the arrival on the Zero-Age-Main Sequence (ZAMS) where the nuclear energy production becomes dominant.

Synthetic HRD consist in generating, from the computed HRD tracks, a theoretical star distribution for a given age, age dispersion and mass distribution. This tool is well suited to study the HRD morphology of observed open clusters, i.e. their main-sequence (MS) extension and width and stellar density in the different regions of the HRD. The synthetic diagrams modify this morphology in function of various factors, namely (i) the initial mass function determining the expected stellar mass distribution, (ii) the age dispersion that establishes the duration of the cluster star formation process and (iii) the binarity rate among the formed stars.

In Sect. 2 we briefly present the new physical ingredients as well as the computed evolutionary sequences. We take advantage of this section to present our isochrones and compare ZAMS location and main sequence width with observations. Sect. 3 is devoted to the synthetic HRD. We first present the method used to generate such distributions, describe the effect engendered by the relevant parameters and test this method to reproduce the morphology of the Pleiades clusters. We finally conclude in Sect. 4.

Let us finally stress that many recent observations clearly outline that PMS stars are accreting matter from a circumstellar disk that could influence the structural evolution during that phase. We are currently investigating that question (see also Bernasconi & Maeder 1996, Siess et al. 1996).

2. HR diagrams: computed models and comparisons with observations

2.1. New PMS models

2.1.1. Physical ingredients

Let us just briefly mention our treatment of quantities that are the most influent as far as PMS and MS phases are concerned.

- Our equation of state is analytic. It includes H, He, C, N and O ionizations. Complete ionization is assumed when $SIX/VIII > 50$. Electrostatic corrections follow the statistical model of Debye-Hückel for partially ionized regions and the Koester (1976) interpolation formula, between the Debye-Hückel and the Thomas-Fermi models, for completely ionized parts. Ionization potentials are also corrected for the continuum depression. Electronic degeneracy is evaluated as soon as its contribution to the total pressure exceeds 0.1%. This formalism is not well suited for very low-mass objects, as explained in Sect. 2.1.3.
- Low-temperature radiative opacities (i.e. below 8000 K) are taken from the new Alexander and Ferguson (1994) tables whereas they were provided by Neuforge (1993) in F94. They are particularly well suited for cool sub-photospheric regions and atmospheres of red sub-giants as they include (i) 59 million molecular lines and (ii) absorption and scattering by dust grains. Among the 35 opacity tables, we first linearly interpolate in $R = \log(\rho/T_6^3)$ and temperature corresponding to each mass shell, and then for its chemical composition (in hydrogen and heavy elements). Above 8000 K, we use the Rogers and Iglesias (1992) opacity tables as in F94. 100 tables were required to obtain accurate enough interpolations (in R , temperature and chemical composition too).
- The stellar structure is integrated from the center to a very low optical depth ($\tau = 0.001$) in the atmosphere. However, at low optical depth (in practice, for $\tau < 10$), the temperature stratification of rather cool stars differ from the Eddington approximated one. We consequently modify the stellar structure equations in that region in order for the temperature gradient and derived quantities (like the radiative gradient and pressure) to correspond to those coming from realistic atmosphere models. More specifically, we use atmosphere models of (1) Plez (1992) for $T_{\text{eff}} < 3900\text{K}$, (2) Eriksson (1995) up to 5500 K. Above that T_{eff} , we computed atmosphere models with the Kurucz program. In the previous computations, F94 was using the stellar atmosphere models of Bell et al. (1975) instead. At each evolution time step (i.e. at each position in the HRD), we search for the atmosphere model corresponding to the T_{eff} , $\log g$ and metallicity Z of the computed stellar surface, by successive linear interpolations between the above mentioned models.
- The structure of convective zones is computed by using the Mixing-Length Theory, following the Kippenhahn et al. (1968) prescription. Our treatment is standard in the sense that no overshooting has been considered. We put $\alpha = 1.5$, rather close to the 1.64 value with which the solar surface properties can be retrieved. Instantaneous mixing has been

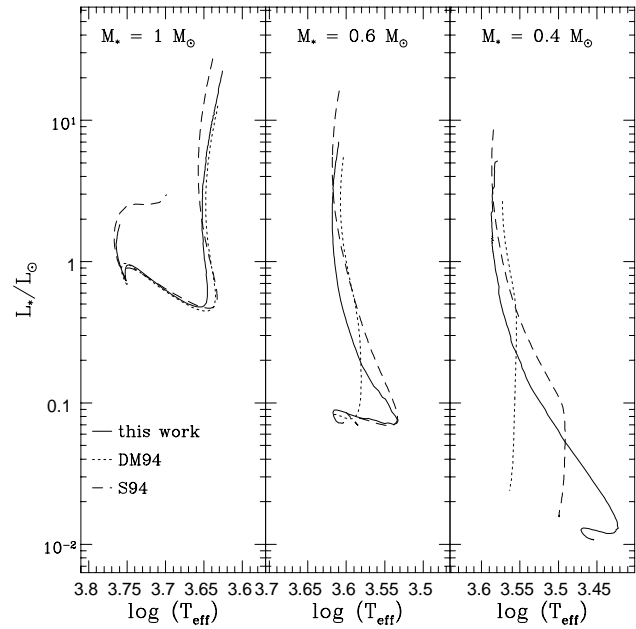


Fig. 1. Comparison between theoretical HRD tracks of 0.4, 0.6 and $1M_{\odot}$ PMS stars computed with different stellar evolution codes

assumed as soon as nuclear transformations occur inside convective regions.

- All the nuclear reaction rates of interest here are coming from Caughlan and Fowler (1988). The weak and intermediate screening factors have been taken into account by using the Graboske et al. (1973) formalism. The evolution of the nuclide abundances is computed by the Wagoner (1969) algorithm.
- Finally, no mass loss has been applied.

2.1.2. Computed models

We computed the early PMS and MS phases of 0.5 to $5M_{\odot}$ stars with $Z = 0.005, 0.02$ and 0.04 , from initially fully convective polytropic models, the central temperature of which is $< 5 \cdot 10^5 \text{K}$. The abundances of heavy elements are scaled from the Anders and Grevesse (1989) elemental distribution. All these models are now available at <http://gag.observ-gr.fr/starevol/evol.html>

Typically 200 to 350 (200 to 700) time steps are required to model the PMS (MS) phase, depending on the total mass. The corresponding number of mass shells ranges between 450 and 600 (550 to 650).

2.1.3. Comparisons with other works

In order to emphasize the key influence of input physics on the resulting surface properties of the modeled stars, we show in Fig. 1 a comparison between HRD tracks obtained by DM94 with the same convection treatment, Swenson et al. (1994, hereafter S94) and us, for three different total masses.

The HRD tracks corresponding to $1M_{\odot}$ objects are very similar. Small differences in the Hayashi track position are mainly due to different treatments of surface conditions (through the atmosphere treatment). On the other hand, ZAMS locations are also very slightly different; this is simply due to small differences in assumed compositions (hydrogen and helium).

At $0.6M_{\odot}$, the DM94 track presents a very reduced radiative part contrarily to ours and those of S94. Also their Hayashi curve is very different. Note however that the S94 evolution path remains comparable to ours.

At $0.4M_{\odot}$, differences are very pronounced, especially below $0.1L_{\odot}$. These are clear signatures of the equation of state. Both DM94 and S94 use equations of state that treat more accurately than us the electrostatic corrections of cool and degenerated matter characteristic of the interior of very low-mass (i.e. $< 0.5M_{\odot}$) objects. This implies that while our track wrongly keeps the same shape, both the DM94 and S94 tracks exhibit a drastic slope change. However, the DM94 path differs from the standard one much earlier in the evolution than the S94 one. This could partly explain the observed difference at $0.6M_{\odot}$ too. Consequently, (i) we will not present tracks for $< 0.5M_{\odot}$ PMS stars as far as our equation of state fails for very low-mass objects and (ii) presently, although PMS tracks computed with different stellar evolution codes for $> 0.5M_{\odot}$ stars almost concur, we stress that there are still large discrepancies at lower masses. This provides an additional motivation to compare theoretical predictions with observations of low-mass stars. Some of these observational constraints will be now reported.

2.2. From theoretical to observational HRD

Special attention has been paid to the transformation from theoretical ($\log L$, $\log T_{\text{eff}}$) to observational (M_V versus (B-V) and M_V versus (V-I)) HR diagram and estimation of associated uncertainties. This transformation involves calibrating the relations T_{eff} -color and T_{eff} -BC and can either be derived from predictions of atmospheric models or from semi-empirical methods.

There is in general a good agreement between predicted bolometric corrections and empirical values (e.g Malagnini et al. 1986 for B-G stars, Leggett et al 1996 for M stars). However a systematic difference between models and observations is observed in the prediction of the (B-V)₀ colors for F-G stars (Arribas & Martinez Roger 1988). Similar discrepancies occur in the prediction of (V-I) colors for M type stars where few direct determinations exist and/or model atmospheres are still uncertain (Leggett et al 1996). We therefore chose to adopt calibration relations derived from empirical or semi-empirical methods.

We adopt the effective temperature scale and bolometric correction compilation of Schmidt-Kaler (1982) for spectral types earlier than K5, the ones of Bessell (1991) for K7 and later. Comparison with the new temperature calibration of Gray & Corbally (1994) does not show systematic differences except in the B star range where these new determinations tend to be lower by $\log T_{\text{eff}} = 0.03$. Typical uncertainties in $\log T_{\text{eff}}$ are thus ≤ 0.02 for A-G stars and $\simeq 0.04$ for O-B and M stars. Bolometric cor-

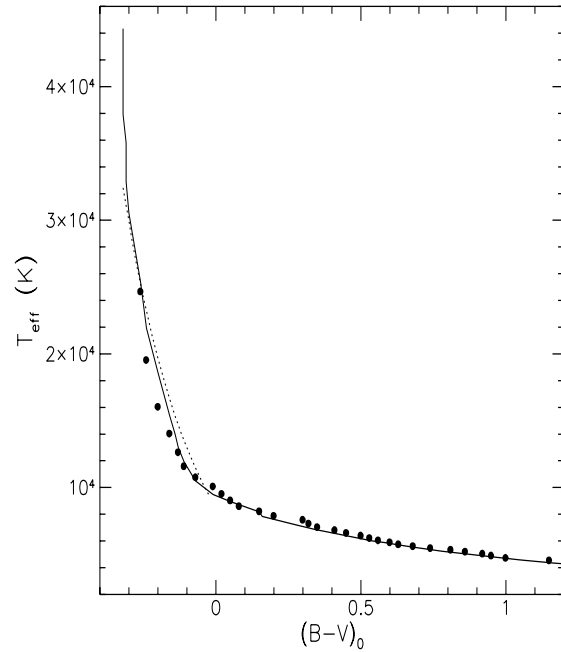


Fig. 2. Recent T_{eff} versus (B-V) calibration relations. We plot in full line the relation compiled in Appendix. Also shown is the empirical determination of Gulati et al. (1989) (dotted line) and the new temperature calibration of Gray and Corbally (1994) combined with (B-V) colors taken from Fitzgerald (1970) (filled circles).

rections have been corrected for zero point differences, assuming $M_{\text{bol},\odot}=4.75$. Adopted values of the bolometric correction agree well with the empirical determination of Malagnini et al (1986), uncertainties being typically 0.2-0.3 magnitudes for K type stars and earlier.

To derive the $T_{\text{eff}}/(B-V)$ conversion, we combine the adopted temperature scale with the (B-V) colors of Fitzgerald (1970), except for temperatures in the range 4000 to 8000 K where we adopt the direct empirical relation derived by Arribas & Martinez-Roger (1988,1989). We compare in Fig. 2 the adopted calibration relation with the one derived from the temperature scale of Gray & Corbally (1994) as well as the one determined by Gulati et al (1989) for O-B stars. We estimate final uncertainties in the location of the tracks in the M_V versus (B-V) diagram to be of the order of 0.02 in (B-V) for $(B-V) \leq -0.05$ and 0.05 for redder values. Uncertainties become much larger for M stars where the (B-V) and BC_V versus T_{eff} relations steepen. We thus restrict ourselves to (B-V) values less than 1.35 and chose to study the low mass range ($T_{\text{eff}} \leq 4000$ K) in the M_V versus (V-I)_C diagram.

(V-I) colors, transformed to the Cousins system as appropriate using the relations given by Bessell (1979), are taken from Bessell (1991) for spectral types K7 and later, Bessell (1979) and Johnson (1966) for earlier spectral types. There is still considerable uncertainty in the determination of a temperature scale for M dwarfs. However, as we saw earlier, this mass range is critical for the study of theoretical pre-main sequence tracks since observed discrepancies between models occur typically

below $0.5M_{\odot}$. There has been for the past years a discrepancy between temperatures derived from modified blackbody fitting methods and the ones obtained through comparison of observed spectral features with predictions from M dwarfs atmospheric models, the latter ones being typically hotter by 200-300 K. This is illustrated in Fig. 3 where we compare the T_{eff} to (V-I) relation adopted in this paper and based on the blackbody temperatures of Bessell (1979, 1991) with the temperature scale of Kirkpatrick et al (1993) derived from the earlier models of Allard (1990). Below 4000 K, discrepancies in the temperature scale lead to differences in (V-I) colors of the order of 0.5-0.6 magnitudes! However, there has been recently considerable improvement in modeling of M dwarf atmospheres which may soon lead to a reconciliation between observations and theory. As illustrated in Fig. 3 the new M dwarf temperatures derived by Leggett (1996) with the most recent atmospheric models of Allard & Hauschildt (1995) lie closer to the blackbody derived ones as well as to theoretical predictions from the model. As is also illustrated in this figure, the calibration of Bessell appears the most compatible with the recent determinations as well as theoretical predictions. Uncertainties in (V-I) colors may however still be as high as $\simeq 0.4$ magnitudes below 4000 K.

All our calibration relations have been derived for solar metallicities, i.e. young-old disk stars. Theoretical models do indeed predict a strong dependence with metallicity, as pointed out by Fig. 3 for the T_{eff} to (V-I) relation. Observations might indicate the same trend although weaker (Leggett et al 1996). Individual measurements are however still too scarce to derive accurate calibrations with different metallicities. Observers should thus be cautious when using these calibrations to derive individual properties of stars.

2.3. The ZAMS location

As a first observational test for our model, we compare in the M_V versus (B-V) diagram the observational ZAMS derived by Mermilliod (1981) with its predicted location from our model. As can be seen in Fig. 4, the agreement is quite good, well within the uncertainties associated with the conversion relations. We also show on this figure the location of the mean main sequence compiled by Schmidt-Kaler (1982) as well as our computed TAMS (Terminal Age Main Sequence) for masses greater than $0.8M_{\odot}$.

In order to test the lower mass end, we compare in Fig. 5 the location in the M_V versus (V-I) $_C$ diagram of the main sequence derived from field stars (Weiss 1984, Leggett 1992) with our predicted ZAMS and TAMS (Terminal Age Main Sequence). Again, there is good agreement between the models and observations. Discrepancy occurs below $0.5M_{\odot}$ where our model systematically lies above the observed main sequence band. It should be noted however that this corresponds to one single mass ($0.4M_{\odot}$) in the model sequence.

Part of this difference could be due to the conversion relations. As we saw above, below (V-I) values of 2.5 uncertainties in the T_{eff} to (V-I) calibration relation are still very large. Most recent determinations would indicate for temperatures below

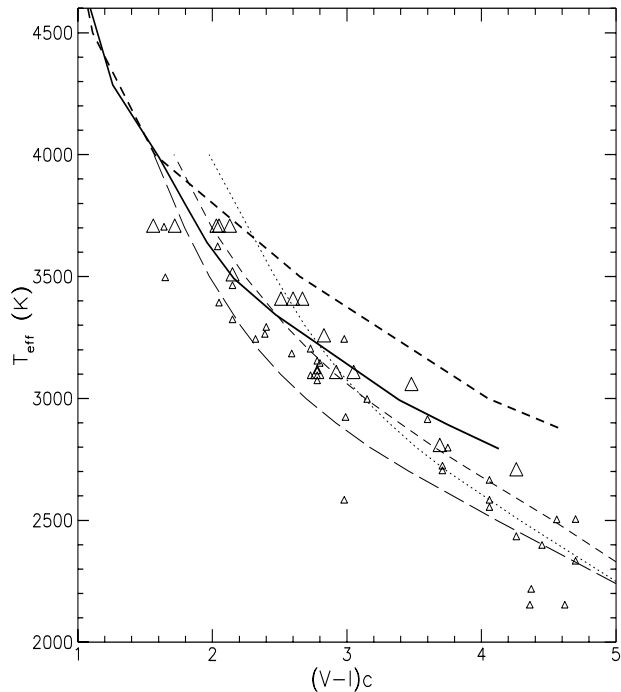


Fig. 3. Recent T_{eff} versus (V-I) $_C$ calibration relations. We plot in thick full line the relation adopted here based on the work of Bessell (1979,1991). For comparison is also shown as a thick dashed line the relation derived by Kirkpatrick et al (1993) from the earlier models of Allard (1990). As thin lines we represent the predictions of the most recent atmosphere models of Allard & Hauschildt (1995): dotted line [M/H]=0, dashed line [M/H]=-0.5, long dashed line [M/H]=-1.5. We also superpose recent individual M dwarfs temperature derivations based on black body methods (small triangles: Berriman et al 1992, Leggett 1992, Jones et al 1994, Tinney et al 1993) and on the comparison of observed spectra with models of Allard & Hauschild 1995 (large triangles: Leggett et al 1996).

3200 K bluer (V-I) colors (by $\simeq 0.4$ magnitudes) than adopted in this work which would bring the observed and predicted main sequence in closer agreement but would not completely solve the discrepancy. Most likely, for these low-mass objects, a better treatment of electrostatic corrections is required which should increase contraction times and lead to a lower luminosity. We will thus below only show our computed models for masses greater than $0.5M_{\odot}$.

2.4. Isochrones and cluster dating

We show in Fig. 6 the theoretical isochrones derived from our work, along with the ones obtained by DM94 and by S94 transformed to the M_V versus (V-I) $_C$ plane with the conversion relations selected above. Although the isochrones appear similar for ages $< 10^7$ yr, there is a significant discrepancy between the models for (V-I) $_0 > 1.5$ and later isochrones. However, these isochrones are very comparable in the turn-over region used to estimate the cluster age. Comparison is made with data for the Pleiades and α Per clusters, extracted from the recent database

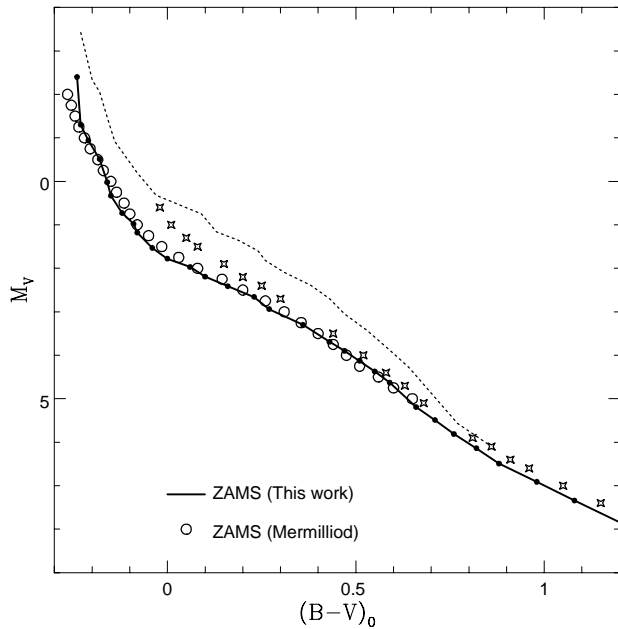


Fig. 4. Predicted versus observed location of the ZAMS in the M_V versus $(B-V)_0$ diagram. The predicted ZAMS derived from our model is shown (full line) with masses ranging from $7M_\odot$ to $0.5M_\odot$ (dots). Superposed is the location of the ZAMS derived from the observation of open clusters by Mermilliod (1981) (open circles). Also represented is our computed TAMS (terminal age main sequence) (dashed line) as well as the mean main sequence location compilation of Schmidt-Kaler (1982) (stars)

compiled by Prosser & Stauffer (1996) based on membership studies. We chose these two clusters for both the size of the photometric sample and their estimated metallicities of $Z \simeq 0.28$ (Boesgaard 1988). Measurements have been transformed from the Kron to the Cousins system using Bessell & Weis (1987) relations. The distance moduli and average reddening assumed for the Pleiades and α Per clusters are $(m - M)_0 = 5.50$ with $A_v = 0.12$ and $(m - M)_0 = 6.10$ with $A_v = 0.30$, respectively. The agreement for all models is good down to $0.6M_\odot$. Below, a systematic deviation from the data points is observed in the isochrones derived from the models of DM94. The 10^8 yr isochrone computed from this work as well as the one derived by S94 on the contrary seem to follow quite well the data points. The discrepancy observed in the DM94 tracks could be due to uncertainties in the adopted calibration relation. However, as noted by Stauffer et al (1995), bringing the DM94 models in closer agreement with the Pleiades data points would require using calibration relations close to the one derived by Kirkpatrick et al (1993). As we saw earlier, more recent determinations seem to imply bluer colors than predicted by this relation. We also cannot fully exclude a gradient in age at the low mass end in the Pleiades. However, taken at face values, the DM94 tracks imply a smooth gradient in age ranging from 10^7 yr at $0.1M_\odot$ to 10^8 yr at $0.6M_\odot$ which seems unphysical.

The age determination of a cluster is generally derived from fits to the upper main sequence turn-off. From Fig. 7 we derive

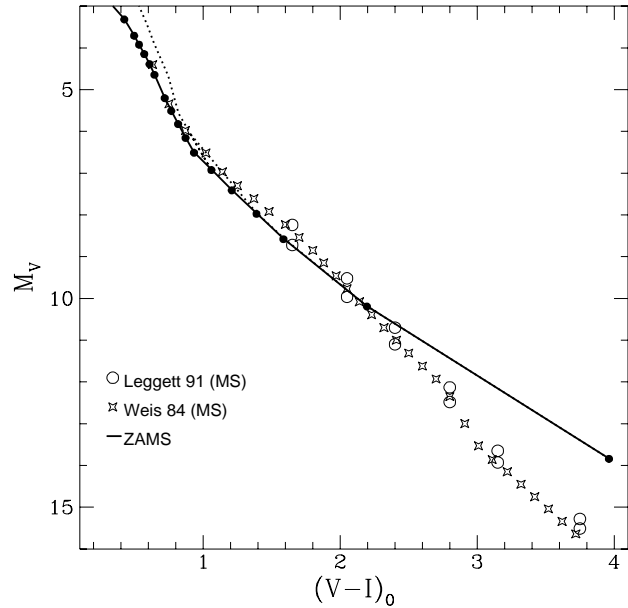


Fig. 5. Comparison of the predicted location of the ZAMS (full line) and TAMS (dashed line) in the M_V versus $(V-I)_0$ with the field stars main sequence band determined by Weiss (1984) (stars) and Leggett (1992) (open circles). For Leggett, the upper/lower point corresponds to young/old disk stars respectively. The TAMS is only shown for masses greater than $1M_\odot$. Dots represent the computed models for masses ranging from 2 to $0.4M_\odot$ by steps of $0.1M_\odot$

an age of order of $4 \cdot 10^7$ yr for α Per. Indeed the $2 \cdot 10^7$ yr isochrone (dotted line) does not match the stellar distribution for low-mass stars whereas the $6 \cdot 10^7$ yr isochrone (dashed line) produces a turn off too early for massive stars. Dealing with the Pleiades cluster, the $5 \cdot 10^7$ yr isochrone can be excluded because it does not match the distribution of low mass stars already located on their ZAMS. The estimated age of the Pleiades is somewhere between $8 \cdot 10^7$ and $1.1 \cdot 10^8$ yr isochrones. Note that the $1.1 \cdot 10^8$ yr isochrone can not account for the more luminous stars in the diagram as they already have moved towards the red giant branch.

With a rather large overshooting given by $d_{over} = 0.20H_p$ (where H_p is the pressure scale height), Meynet et al. (1993) found ages of order of $5.2 \cdot 10^7$ and 10^8 yr for these two clusters, respectively. As the exact amount of overshooting required for intermediate-mass objects during central H burning is still very undetermined, this introduces an age indetermination of about 20% for α Per cluster. For the Pleiades, the age determination is comparable or somewhat lower than estimates including overshooting. Note that our predicted width of the main sequence band ($\Delta M_V \sim 1.5$ in Fig. 4) compared to the value of 2 magnitudes derived by Jaschek and Mermilliod (1984) in the A type star domain [$-0.05 < (B-V)_0 < 0.4$] is in favor of a moderate overshooting in intermediate-mass stars.

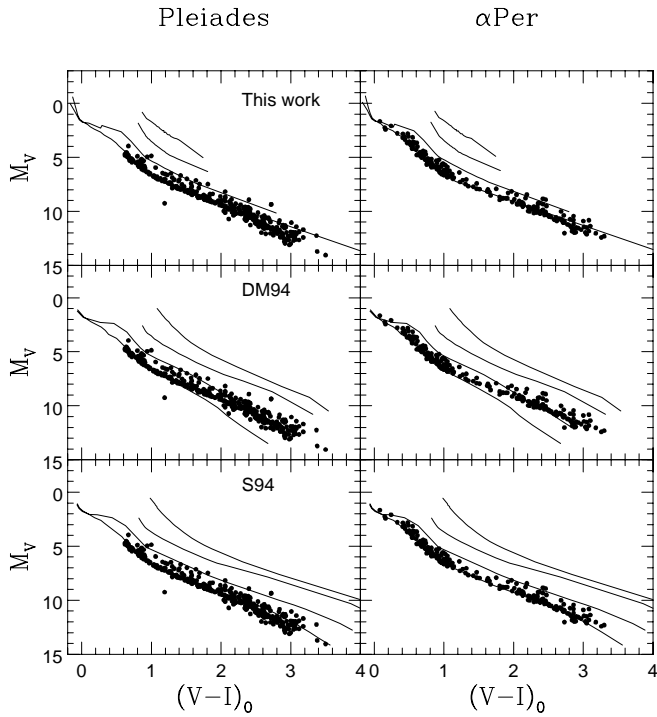


Fig. 6. Comparison between the isochrones of different evolutionary tracks transformed into the observational M_V versus $(V-I)_0$ plane and data for the Pleiades and α Per clusters. The considered masses range from 5 to $0.5M_\odot$. For the DM94, the star masses range from 2.5 to $0.1M_\odot$, while for S94 they range from 5 to $0.15M_\odot$. From upwards, the isochrones correspond to ages of 10^5 , 10^6 , 10^7 and 10^8 yr, respectively. Data points have been extracted from Prosser & Stauffer (1996)

3. Synthetic HRD and comparison with standard clusters

3.1. The overall problem

Given an initial mass function and a star formation rate function, we intend to estimate the number of stars with ages ranging in the interval $[t, t + dt]$ and mass interval $[m, m + dm]$. In this model, we adopt a gaussian SFR and restrict its domain of integration to the interval $[t_1, t_2]$. Stars are also supposed to be formed with masses ranged between m_{inf} and m_{sup} ¹. So, the number of stars dn_t born between t and $t + dt$, is given by

$$dn_t = A_t e^{-\frac{(t-t_0)^2}{2\sigma_t^2}} dt, \quad (1)$$

where t_0 is the estimated age of the cluster and A_t the normalization constant such that

$$\int_{t_1}^{t_2} dn_t = n_{star},$$

where n_{star} is the population of the cluster.

The first stage of the procedure consists in dividing the interval $[t_2 - t_1]$ in p bins of identical width Δt ($t_i = t_1 + i\Delta t$).

¹ The values of m_{inf} and m_{sup} are fixed by the extent of our grid, i.e. $0.5M_\odot$ and $5M_\odot$, respectively

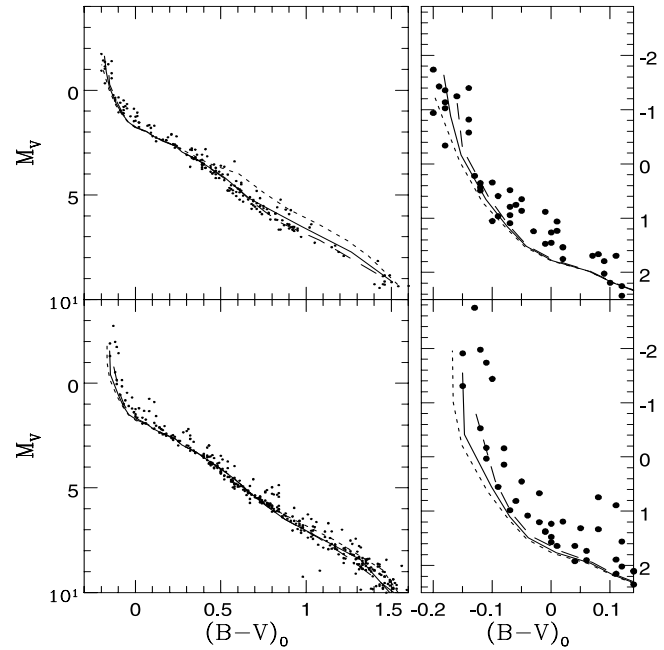


Fig. 7. Dating of the Pleiades (lower) and α Per (top panel). Data have been extracted from the Prosser & Stauffer database. The dotted, solid and dashed lines correspond to ages of $2 \cdot 10^7$, $4 \cdot 10^7$ and $6 \cdot 10^7$ yr for α Per and $5 \cdot 10^7$, $8 \cdot 10^7$ and $1.1 \cdot 10^8$ yr for the Pleiades, respectively. Symbols are as in Fig. 6

The number of stars n_i contained in bin i is then given by the integration of Eq.(1) over the interval $[t_i, t_i + \Delta t]$.

3.1.1. The transformation method

The question now is to determine what will be the mass of each star in each bin of time, given the chosen IMF. To answer this question, let us remind that if x and y are random variables with respective probability distribution $f(x)$ and $g(y)$, the fundamental transformation law of probabilities tells us that $|f(x)dx| = |g(y)dy|$ or

$$g(y) = f(x) \left| \frac{dx}{dy} \right|. \quad (2)$$

Computers generate random numbers with a uniform probability distribution, i.e. with $f(x) = 1$. The problem now boils down to solve the differential equation $dx/dy = g(y)$ which solution is just $x = \int g(y) = F(y)$. Therefore, the desired transformation that takes a uniform distribution into one distributed as $g(y)$ is

$$y(x) = F^{-1}(x), \quad (3)$$

where F^{-1} is the inverse function of F . As a consequence, this method requires that function g is analytic. This is the case because, in our context, variable y and function g represent the stellar mass and IMF, respectively.

3.1.2. The Initial Mass Function

For each star born in an interval Δt , we sort a uniformly distributed number x . Then, the corresponding mass m is given by the requirement that $x = \int_{m_{inf}}^m \text{IMF}(m') dm'$. For our purposes, we have tried three different prescriptions for the IMF, namely

- a single power law of the form

$$\frac{dn_m}{dm} = A_o m^{\gamma_0},$$

corresponding to the Salpeter (1955) law. The normalization constant A_o is determined so that $\int_{m_{inf}}^{m_{sup}} A_o m^{\gamma_0} dm = 1$ and the exponent $\gamma_0 = -2.35$

- a multiple power law

$$\frac{dn_m}{dm} = \begin{cases} A_1 m^{\gamma_1} & \text{if } m_{inf} \leq m \leq m_1 \\ A_2 m^{\gamma_2} & \text{if } m_1 \leq m \leq m_2 \\ A_3 m^{\gamma_3} & \text{if } m_2 \leq m \leq m_{sup}. \end{cases}$$

Constants A_1 to A_3 are constrained in order to normalize the global function to unity and ensure its continuity. From observations of the distribution of low-mass stars in the Galactic disk, Kroupa et al. (1993) found that $\gamma_1 = -1.3$, $\gamma_2 = -2.2$ and $\gamma_3 = -2.7$, with m_1 and m_2 equal to 0.5 and $1.0M_{\odot}$, respectively.

- and finally a log-normal distribution

$$\frac{dn_m}{d\log m} = A_m e^{-\frac{(\log m - \log m_o)^2}{2(\log \sigma_M)^2}}, \quad (4)$$

which has been proposed by Strom et al. (1993) as an analytic approximation of the field IMF derived by Scalo (1986). The fitting parameters are $\log m_o = -0.54$ and $\log \sigma_M = 1.1$. As usual, A_m normalizes the distribution to unity.

In all our calculations, we have assumed a constant IMF in the interval $[t_1, t_2]$.

3.1.3. The binarity rate

The stellar population of a cluster is composed of a large fraction of photometric and spectroscopic binaries and this important component has been taken into account in our simulations. We assume a uniform mass ratio distribution. The binary proportion p_b is a free parameter. The problem consists in determining the effective mass ratio. First of all, for each star i (with mass m_i), we sort a random number x . If the condition $x \leq p_b$ is satisfied, the star belongs to a binary system. In that case, a second number y is sorted that will give the mass ratio r_i in the appropriate distribution by the transformation method described in Sect. 3.1.1. We only take into consideration however companions with masses greater than $0.5M_{\odot}$. The HRD coordinates of the resulting companion, aged of $t_i + \Delta t/2$ and with a mass $m_c = r_i m_i$, are then determined. Finally, the binary is placed in the HRD, so that

$$\begin{aligned} L &= L_1 + L_2 \\ T_{\text{eff}} &= \frac{T_{\text{eff},1} L_1 + T_{\text{eff},2} L_2}{L_1 + L_2}, \end{aligned}$$

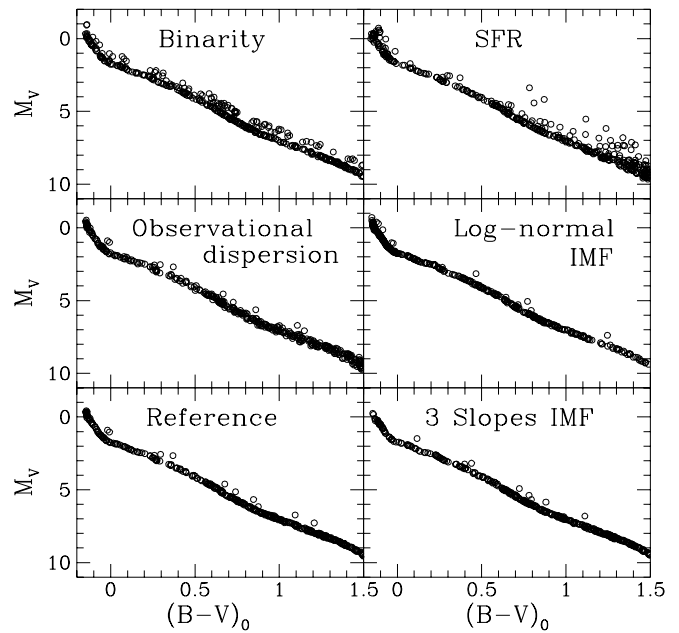


Fig. 8. Effects of varying binary proportion, SFR, IMF and observational uncertainties on a synthetic HRD in the $(B-V, M_V)$ plane. The reference synthetic diagram is shown in the lower left panel. At its right, the Salpeter's IMF is replaced with the multiple power law, while in the intermediate right panel, it is replaced by the log-normal IMF. In the intermediate left panel, the observational uncertainties have been added. In the upper left panel the proportion of binaries is increased to $p_b = 0.5$ and to its right the star formation duration enhanced to $\sigma_t = 3 \cdot 10^7$ yr

where suffixes 1 and 2 refer to the primary and secondary components, respectively.

3.1.4. Observational uncertainties

The effective temperature and luminosity of a given star are linearly interpolated in our grids of models but before appearing in the final synthetic HRD, we have simulated the uncertainties introduced by the observations themselves. To do this, we add to the effective temperature T_{eff} an uncertainty ΔT_{eff} given by $\Delta T_{\text{eff}} = (x_{\Delta} - 1/2)\Delta T$, where x_{Δ} a random number uniformly distributed in $[0, 1]$ and

$$\Delta T = \begin{cases} 2\sigma_T \left(\frac{4000 \text{ K}}{T_{\text{eff}}}\right)^2 & \text{if } \Delta T > 50\text{K}, \\ 50\text{K} & \text{if } \Delta T < 50\text{K}, \end{cases}$$

with σ_T a free parameter. The function ΔT has been built in order to reproduce a larger uncertainty attached to the determination of T_{eff} in cool stars that justifies the power 2. For $\sigma_T = 100\text{K}$, this leads to a mean uncertainty of 100 K for stars with $T_{\text{eff}} \simeq 4000\text{K}$, an error generally accepted for T Tauri stars. This uncertainty decreases to $\sim 50\text{K}$ for stars with $T_{\text{eff}} \simeq 8000\text{K}$.

Similarly, we generate a dispersion $\Delta M_{\text{bol}} = (x_{\Delta} - 1/2)\Delta M_b$ on the absolute bolometric magnitude M_{bol} where ΔM_b is arbitrary fixed to 0.05.

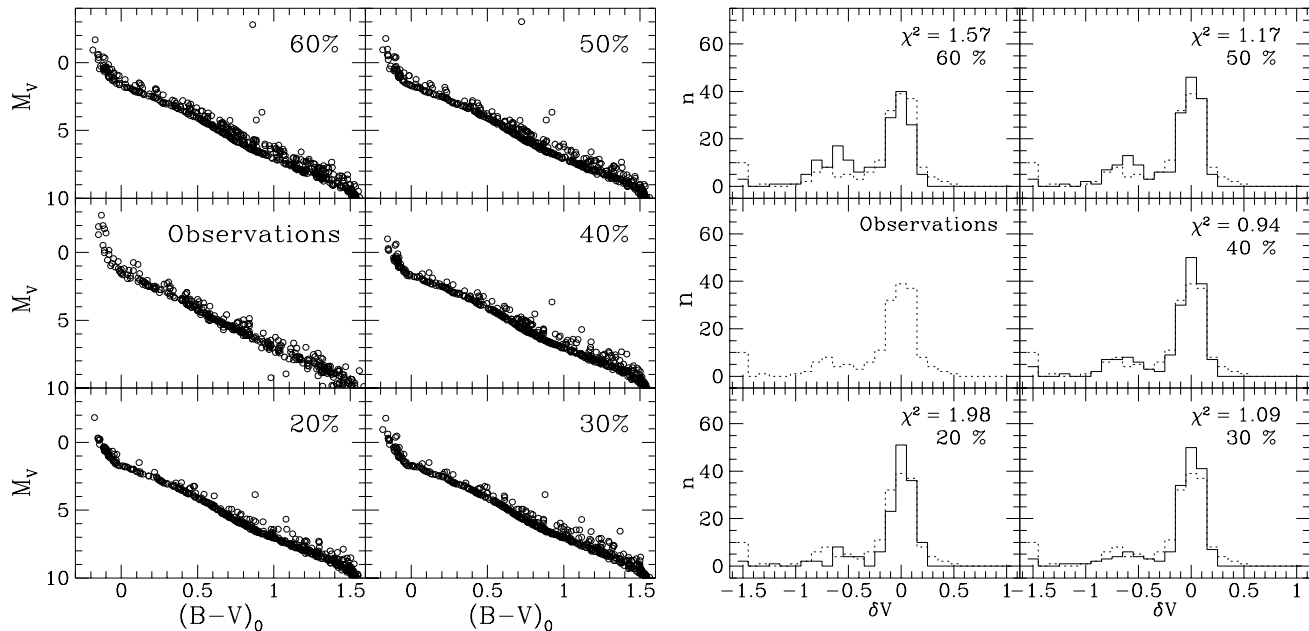


Fig. 9. Left panel: synthetic HR diagrams for the Pleiades for different binarity rates compared to the observed HRD. Right panel: histograms counting stars in cells around the ZAMS in the central region of the color-magnitude diagram delimited by $2.5 \lesssim M_V \lesssim 6.5$ and $0.2 \lesssim (B-V) \lesssim 0.9$, for the different binarity rates invoked in the left panel. The dashed histogram represents the Pleiades data and the solid histogram the model for different binary proportions. The reduced χ^2 value is indicated in each panels. From this figure we conclude that the binary proportion in the Pleiades is somewhat between 30 and 40%

3.2. Influence of the parameters

We investigate in Fig. 8 the influence of the different parameters, namely the IMF, the SFR, the observational uncertainties and the binary proportion. The synthetic cluster is composed of 400 stars and aged of $t_0 = 8 \cdot 10^7$ yr. In the reference case, default parameters are $p_b = 0.1$, $\sigma_t = 5 \cdot 10^6$ yr, the IMF is the Salpeter's one, and observational uncertainties are absent.

The binary proportion affects the general shape of the distribution because it introduces a second band detached from the t_0 isochrone that results from the composite luminosity and effective temperature of the binary system. The widening is present at all masses and allows to populate the upper left of the diagram.

The age dispersion greatly modifies the synthetic HRD by spreading stars around the t_0 isochrone. Indeed, the last formed low-mass stars are still on their Hayashi track and exhibit a wide range of luminosities. The effect is particularly marked for $(B-V) > 0.7$, i.e. for stars less massive than $0.9 M_\odot$. A larger σ_t also leads to a widening of the MS band of massive stars as some of them have already enough time to depart from their ZAMS.

The observational uncertainties mainly operate on low-mass stars where they introduce a noticeable widening of the distribution. Massive stars are weakly affected by these errors.

Finally, we compare the three IMF. Due to the large σ_M comparable to the mass range entering our simulations ($0.5 M_\odot < M < 5 M_\odot$), the log-normal distribution is very flat and almost uniformly distributes stars in the synthetic diagram. The three slope IMF looks like the Salpeter's one because very low-mass stars are absent. Indeed, these laws are very similar above

$0.5 M_\odot$. We just notice a smaller density of massive stars in the three slope IMF, a consequence of $\gamma_3 > \gamma_0$.

We note that the various parameters introduced in the synthetic HRD have specific effects that affect differently its morphology. They consequently can be constrained by the observed HRD.

3.3. Application to the Pleiades

In very young clusters, the spread in luminosity in the HRD is too important to show the net effects of parameter changes. We consequently restrict this study to open clusters composed of stars located close to their ZAMS. We chose to test first our method on the well-studied Pleiades cluster, where selection effects should be minimized. We also focus on the M_V versus $(B-V)$ diagram because of our cut-off in mass at $0.5 M_\odot$.

Recently Goldberg and Mazeh (1994) suggested that the mass ratios of the binaries present in the Pleiades cluster are rather uniformly distributed. The study of Mermilliod et al. (1992) also supports this point of view. Assuming that, we will try to use synthetic HRD in order to give estimates of binary fraction in this cluster.

The presented synthetic HRD in Fig. 9 have been obtained with the $Z = 0.02$ grid of evolutionary models, suitable for the Pleiades. The IMF with which we best fit the Pleiades data is the multiple power law. Indeed, the log-normal distribution seems to lead to a relatively higher number of massive stars, inconsistently with observations. This probably results from the very large mass dispersion σ_M invoked in Eq. (4). However, because

Table 1. Adopted calibration relations for solar metallicities dwarf stars

$\log T_{\text{eff}}$	BC_V	$(B-V)_J$	$(V-I)_C$
4.648	-4.28	-0.32	-0.34
4.613	-3.81	-0.32	-0.34
4.580	-3.56	-0.32	-0.34
4.555	-3.43	-0.31	-0.34
4.518	-3.21	-0.31	-0.34
4.486	-3.04	-0.30	-0.3
4.405	-2.58	-0.26	-0.26
4.342	-2.23	-0.24	-0.23
4.271	-1.82	-0.20	-0.19
4.188	-1.34	-0.16	-0.16
4.146	-1.09	-0.14	-0.14
4.115	-0.90	-0.13	-0.12
4.077	-0.68	-0.11	-0.09
4.022	-0.39	-0.07	-0.05
3.978	-0.18	-0.01	-0.02
3.965	-0.11	0.02	0.02
3.953	-0.08	0.05	0.07
3.914	-0.03	0.15	0.15
3.895	0.00	0.16	0.25
3.857	0.03	0.28	0.33
3.838	0.01	0.34	0.42
3.809	-0.02	0.44	0.52
3.792	-0.04	0.50	0.59
3.780	-0.06	0.54	0.62
3.768	-0.08	0.59	0.67
3.760	-0.09	0.62	0.69
3.746	-0.13	0.67	0.75
3.720	-0.19	0.78	0.82
3.690	-0.30	0.92	0.94
3.662	-0.43	1.05	1.11
3.638	-0.60	1.17	1.26
3.602	-0.98	1.36	1.6
3.580	-1.21	1.41	1.8
3.562	-1.39	1.48	1.96
3.544	-1.61	1.52	2.16
3.525	-2.03	1.55	2.47
3.498	-2.56	1.60	2.86
3.477	-3.34	1.82	3.39
3.462	-3.83	1.94	3.75
3.447	-4.43	2.06	4.13
3.431	-5.10		4.5
3.415	-5.50		4.5

of the possible influence of some sample incompleteness, firm conclusion cannot be drawn concerning the IMF choice.

We further assume $\sigma_T = 100\text{K}$ for the observational uncertainties. As σ_t mainly affects the width of the low-mass stars distribution above the ZAMS, a rather large value of this parameter ($\sigma_t \simeq 3 \cdot 10^7 \text{ yr}$) has been required to reproduce the observed width. Our simulations are shown in Fig. 9. The number of stars in the sample and the simulations is of order of 400. From a first visual inspection of the figure, we see that a relatively high (> 20%) proportion of binaries is required to account for the star density of the second band above the ZAMS. On the contrary a binary proportion above 50% is excluded because it populates too much this second band. Finally, it is difficult to reproduce

the more luminous stars but this problem could be related to the absence of overshooting in our stellar models.

To evaluate more precisely the general conclusion drawn above, we have constructed an histogram that represents the distribution of stars perpendicular to the ZAMS. We concentrate on A7-K1 stars in the color range $0.2 \lesssim (B-V) \lesssim 0.9$ ($2.5 \lesssim M_V \lesssim 6.5$), where the sample (179 stars) is supposed to be reasonably complete and where the ZAMS can be linearly approximated by

$$M_V = 5.87(B-V) + 1.26 .$$

This region is further subdivided by lines running parallel to the ZAMS but offset by a constant δV . The color-magnitude diagram data are counted into these cells and compared to the observed distribution with a χ^2 test. We see in Fig. 9 that the best fit is obtained for a binarity fraction of $40\% \pm 5\%$. We stress that our approach allows us to estimate the true binary fraction given a mass ratio distribution. More specifically we are sensitive to all mass ratios and separation provided both stars are more massive than $0.5M_\odot$. We thus count the binaries located within the “single” star main sequence as well. Our derived fraction is consistent with the 34% determined by Mermilliod et al. (1992) in the Pleiades for F-G stars, from a combined photometric and spectroscopic analysis. It also compares quite well with the main sequence G dwarf binary fraction of 44 % derived by Duquennoy & Mayor (1991).

4. Conclusions

We compute the early PMS and MS phases of 0.4 to $5M_\odot$ stars with $Z = 0.005, 0.02$ and 0.04^2 . We compare our models with those provided by DM94 and S94 and we showed important deviations in PMS tracks for stellar masses below $0.5M_\odot$, most probably due to differences in the treatment of electrostatic corrections in cool degenerated matter.

Special attention has been paid to the conversion relations from theoretical ($\log L, \log T_{\text{eff}}$) HRD to observational (magnitude-color) diagrams. We adopted calibration relations based on empirical methods. Uncertainties are still large in the O-B and M star domains.

Comparison between our predicted and observed location of the ZAMS and TAMS in the M_V versus (B-V) and M_V versus (V-I) diagrams is very good for masses above $0.5M_\odot$. Discrepancy observed below cannot be fully accounted for by the uncertainties in the color to temperature conversion relations and could be due to our improper treatment of electrostatic corrections for such low-mass objects. In the M_V versus (V-I) diagram, our 10^8 yr isochrone is in good qualitative agreement with the low-mass end distribution of the Pleiades and $\alpha \text{ Per}$ clusters.

From the M_V versus (B-V) turn-off, we find ages of $4 \cdot 10^7$ for $\alpha \text{ Per}$ cluster and between $8 \cdot 10^7$ and 10^8 yr for the Pleiades cluster. These ages are somewhat lower than previous determinations including overshooting contrary to us.

² Now available at the WWW address:

<http://www-laog.obs.ujf.-grenoble.fr/liens/starevol/evol.html>

We generate synthetic HRD diagrams including different IMF, star formation rates and accounting for binary stars and observational uncertainties. The synthetic HRD diagrams prove to be a useful tool to study the morphology of young clusters and constrain the above-mentioned parameters. We apply this procedure to the Pleiades cluster. We best reproduce its morphology with an age dispersion of $3 \cdot 10^7$ yr and a fraction of binary systems with companion mass greater than $0.5M_{\odot}$ for F-G stars of $40\% \pm 5\%$. We also favor the multiple power law IMF but we cannot clearly discriminate at this point between different IMF relations because of possible incompleteness of observational data.

Acknowledgements. First of all, we thank D. Alexander and K. Eriksson for providing us with new opacity tables and cool atmosphere models, respectively. We are also grateful to D. C. Prosser for making his database on open clusters available to us prior to publication. We also wish to thank the anonymous referee for constructive comments which have improved this paper. Part of the computations presented in this paper were performed at the “Center de Calcul Intensif de l’Observatoire de Grenoble”. Most of them have been realized at “IMAG” on a IBM SP1 computer financed by the MESR, CNRS and Région Rhône-Alpes.

Appendix A: calibration relations (see Table 1)

References

- Alexander, D. R., Ferguson, J. W. 1994, ApJ, 437, 879
 Allard, F. 1990, Ph.D. thesis, Rupert Karls Universitat Heidelberg
 Allard, F., Hauschildt, P.H., 1995, ApJ, 445, 433
 Anders, E., Grevesse, N. 1989, Geochim. Cosmochim. Acta, 53, 197
 Arribas, S., Martinez Roger, C. 1988, A&A, 206, 63
 Arribas, S., Martinez Roger, C. 1989, A&A, 215, 305
 Bell, R.A., Eriksson, K., Gustafsson, B., Nordlund, A.: 1975, A&AS, 23, 37
 Berriman, G.B., Reid, N., Leggett, S.K. 1992, ApJ, 392, L31
 Bessell, M.S. 1979, PASP, 91, 589
 Bessell, M.S. 1991, AJ, 101, 662
 Bessell, M.S., Weis, E.W. 1987, PASP, 99, 642
 Bodenheimer, P. 1965, ApJ, 142, 451
 Boesgaard, A.M. 1988, ApJ, 336, 798
 Caughlan, G.R., Fowler, W.A. 1988, Atomic Data Nucl. Data Tables, 40, 283
 D’Antona, F., Mazzitelli, I. 1984, A&A, 138, 431
 D’Antona, F., Mazzitelli, I. 1994, ApJS, 90, 467
 Duquennoy, A., Mayor, M. 1991, AA, 248, 485
 Eriksson, K. 1995, private communication
 Fitzgerald, M.P. 1970, A&A, 4, 234
 Forestini, M. 1994, A&A, 285, 473, F94
 Goldberg D., Mazeh T. 1994, A&A, 282, 801
 Graboske, H.C., DeWitt, H.E., Grossman, A.S., Cooper, M.S. 1973, ApJ, 181, 457
 Gray, R.O., Corbally, C.J. 1994, AJ, 107, 742
 Gulati, R.K., Malagnini, M.L., Morossi, C. 1989, A&AS, 80, 73
 Iben, I. 1965, ApJ, 141, 693
 Jaschek C., Mermilliod J.C. 1984, A&A, 137, 358
 Johnson, H.L. 1966, ARAA, 4, 193
 Jones, H.R.A., Longmore, A.J., Jameson, R.F., Mountain, C.M. 1994, MNRAS, 267, 413
 Kippenhahn, R., Weigert, A., Hofmeister, E. 1968, Methods of Computational Physics, 7, 129
 Kirkpatrick, J.D., Douglas, M.K., Rieke, G.H., Liebert, J., Allard F., Wehrse, R. 1993, ApJ, 402, 643
 Koester, D. 1976, A&A, 52, 415
 Kroupa, P. Tout, C.A., Gilmore, G. 1993, MNRAS, 262, 545
 Leggett, S. K. 1992, ApJS, 82, 351
 Leggett, S.K., Allard F, Berriman, G., Conard, C.D., Hauschildt, P.H. 1996, ApJS, 104, 117
 Malagnini, M.L., Morossi, C., Rossi, L., Kurucz, R.L. 1986, A&A, 162, 140
 Mazzitelli, I. 1989, in ESO Conf. Proc. 33 “Low-Mass Star Formation and Pre-Main Sequence Objects”, ed. B. Reipurth (Garching, ESO), 433
 Mermilliod J.-C. 1981, A&A, 97, 235
 Mermilliod J.-C., Rosvick J.M., Duquennoy A., Mayor M. 1992, A&A, 265, 513
 Meynet, G., Mermilliod, J.-C., Maeder, A. 1993, A&AS, 98, 477
 Neuforge, C. 1993, A&A, 268, 650
 Plez, B. 1992, A&AS, 94, 527
 Proffitt, C.R., Michaud, G. 1989, ApJ, 346, 976
 Prosser, C.F., Stauffer, J.R. 1996, Open Cluster Database, priv. comm.
 Rogers, F.J., Iglesias, C.A. 1992, ApJS, 79, 507
 Ryan, S.G., Norris, J.E., Bessel, M.S., Deliyannis, C.P. 1992, ApJ, 388, 184
 Salpeter, E.E. 1955, ApJ, 121, 161
 Scalo, J.M. 1986, Fundamentals of Cosmic Physics, vol. 11, 1
 Schmidt-Kaler, 1982, Physical parameters of the Stars, in Landolt-Bornstein New Series, Vol 2b, astronomy and astrophysics - stars and star clusters (eds. K. Schaifers, H.H. Voigt). New-York: Springer-Verlag.
 Stauffer, J.R., Hartmann, L.W., Barrado, D., 1995, ApJ, 454, 910
 Strom, K.M., Strom, S.E, Merrill, K.M. 1993, ApJ, 412, 233
 Swenson, F.J., Faulkner, J., Rogers, F.J., Iglesias, C.A. 1994, ApJ, 425, 286
 Wagoner, R.V. 1969, ApJS, 162, 247
 Tinney, C.G., Mould, J.R, Reid, I.N., 1993, AJ, 105, 1045
 Trimble, V.L., Ostriker, J.P. 1978, A&A, 63, 433
 Weis, E.W. 1984, ApJS, 55, 289